Synthesis and Characterization of Se-doped ZnO Nanoparticles by Electrochemical Method: Photodegradation Kinetics of Indigo Carmine Dye and Study of Antimicrobial, Antimitotic Activities of Se-doped ZnO Nanoparticles

Sowbhagya[1] and Sannaiah Ananda[1*]

[1]*Department of Studies in Chemistry, Manasagangotri, University of Mysore, Mysore-570 006, India.*

Authors' contributions

This work was carried out in collaboration between both authors. Both authors read and approved the final manuscript

Original Research Article

ABSTRACT

In the past few decades selenium nanoparticles have received a considerable importance because of its effective biological applications. Therefore, nano-structured Se-doped ZnO photocatalyst has been synthesized by electrochemical method, which is a simple and an inexpensive method. The characterization techniques included are UV-Visible spectroscopy, IR spectroscopy, SEM and X-ray diffraction techniques. From UV-Vis spectroscopy and by using Tauc plot the band gap energy of Se-doped ZnO nanoparticles is calculated and is found to be 2.6eV. The IR spectra showed the peak at 427 cm^{-1} for ZnO bonds and peaks at 518cm^{-1}, 612cm^{-1}, 727cm^{-1} and 1373cm^{-1} correspond to the presence of Se-ZnO bending and stretching vibrations. From the XRD data and with the help of Williamson-Hall plot the crystalline size is calculated and it is found to be ~25.5 nm. The photocatalytic activity of the synthesized Se-doped ZnO nanoparticles was investigated by the kinetics of degradation of Indigo carmine dye. The degradation efficiency of Se-doped ZnO was found to be ~96%. The antimicrobial and antimitotic activities were evaluated for the synthesized ZnO and Se-doped ZnO nanoparticles against the control.

Corresponding author: Email: snananda@yahoo.com;

1. INTRODUCTION

In the recent years nanotechnology has become one of the promising tools for scientific innovations. Metal nanoparticles have found many applications in medicine, electronics and in many industries [1-3], because of their unique, electronic, optical, catalytic and magnetic properties [4-7]. Catalysis using metal oxide nanoparticles is currently a subject of great interest and intensive research is being carried out to ensure the biological applications.

Consequently a growing interest in heterogeneous Photocataysis as an advance oxidation technique has been developed. The use of nano semiconductors as photocatalyst and as biological agents, to initiate redox reactions, have generated great interest due their unique physiological properties, caused by nanosized dimensions and large surface/volume ratios. ZnO has emerged to be more efficient catalyst as for as water detoxification is concerned because it generates more number of H_2O_2 efficiently and it higher rate rate mineralization. Also, it has more number of active sites with high surface activity [8]. Among the various semiconducting materials, although TiO_2 is extensively investigated and wildly employed, some studies have highlighted that ZnO exhibits better efficiency than TiO_2 for removing organic compounds in water bodies and photoelectric conversion. Studies have showed that ZnO nanoparticles can also be used as an antimicrobial agent.

Doping metal ions into ZnO can influence the performance of these photocatalysts. This affects the dynamics of electron: Hole pair recombination and interfacial charge transfer. The largest enhancement of photoactivity through doping can be found in nano sized particles. Selenium is a trace element, very essential for normal health and reproduction. It was considered as a poison until it was identified as a micronutrient for bacteria, mammals and birds. Selenium is essential for the effective operation of the immune system in both animals and humans. It has received considerable attention because of its remarkable biological applications such as anticancer, antimicrobial, antidiabetic and antioxidant activities [9-13]. Research is under progress to extract the medicinal applications of selenium nanoparticles such as anticancer, antimicrobial [14], orthopaedic or malignant mesothelioma. Results from epidemiological, ecological clinical studies have shown se decreases the risk of some cancers such as prostate, lung and colon cancers [15-17]. Selenium nanoparticles are also known for their remarkable applications such as photodegradation, photoconductivity and wastewater treatment. Many nanoparticles are known for their anti cancer application for example silver nano particles. But silver nanoparticles (the group of Prof. Barcikowski) can cause damage to human tissue in such case selenium nano particles can be used. Here we have doped Selenium to ZnO in order to enhance the activity of Selenium. Keeping all these view in mind Selenium is selected for doping with ZnO.

Further, in order to synthesis these nanoparticles, the development of simple and reliable methods is very essential. In this way, electrochemical method for the synthesis of Se-doped ZnO nanoparticles plays a very important role, which is simple, easy to handle, reliable and an inexpensive method.

Dyes are important organic pollutants and their release as waste water in the eco-system causes pollution and perturbation to aquatic life. Photocatalytic degradation for the purpose of purifying waste water from industries and households has attracted attention in the recent years [18]. Therefore the removal of these hazardous materials from water bodies is very

important. Using Se-doped ZnO nanoparticles one can remove these hazardous materials from water sources up to ~96%. The coating of an insulating layer on TiO_2 particles enhances the photocatalytic activity has been reported [19].

In this way electrochemical method offers a green technology for the synthesis of metal oxide nanoparticles, which is an environmentally friendly method.

2. EXPERIMENTALS

2.1 Synthesis of Se-doped ZnO Nanoparticles by Electrochemical Method

The experimental set up is as shown in Fig. 1. The metal wire (Zn) is used as anode and platinum electrode is used as cathode. Using 30 mA current and potential of 12 V the experiment was run for 3 hrs with continuous stirring. The electrolytic cell is consisting of 0.05 g of Na_2SeO_3 and 0.5 % of aqueous $NaHCO_3$ solution. 1cm gap between electrodes is maintained. During the electrolysis the zinc electrode which acts as anode starts to dissolve and gives zinc ions which are electrochemically reacted with $NaHCO_3$ and Na_2SeO_3 to give Zn (II) oxide/Hydroxide with selenium. The solid obtained was then washed with double distilled water till complete removal of $NaHCO_3$. Since the melting point of Se is 210^0C, heating to higher temperature is avoided, so the wet powder was then heated at 180^oC for dehydration and removal of hydroxides to get Se-doped ZnO nanoparticles. The synthesis takes place at electrode-electrolyte interface or close to the electrode within the electrical double layer [20]. The product is deposited on the surface of the electrode in the form of a thin film or coating and it also floats on the solution which is collected by filtration [21]. The pH of the solution before electrolysis and after electrolysis was found to be alkaline. Since the redox potential of Zn (-0.77) and Se (-0.37) is different, the rate of electrochemical reaction will not be same. Since the dissolution potential of Zn is more negative than selenium and selenium oxide dissolves in water, it is expected that the selenium present in the solution will be doped in ZnO. Hence the mechanism for the synthesized ZnO and Se-doped ZnO nanoparticles is given in scheme 1.
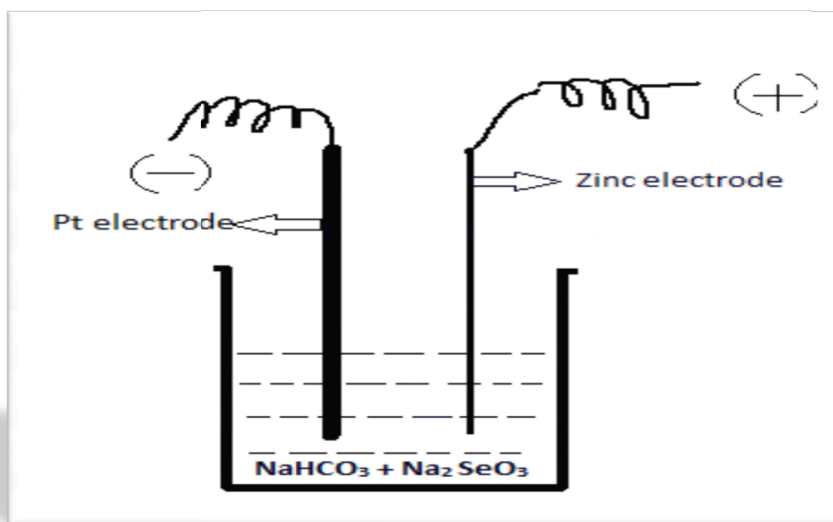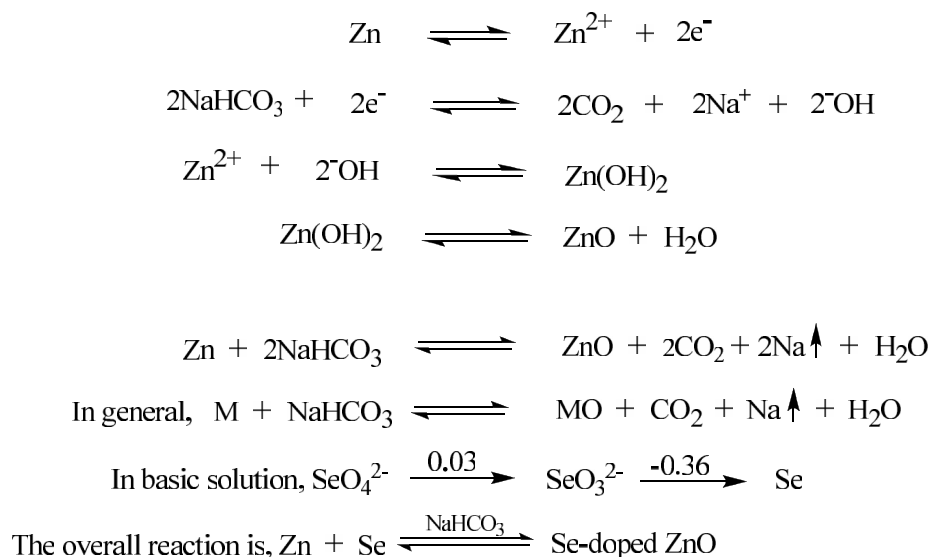

Fig. 1. Experimental set up for the synthesis of Se-doped ZnO nanoparticles

$$Zn \rightleftharpoons Zn^{2+} + 2e^-$$

$$2NaHCO_3 + 2e^- \rightleftharpoons 2CO_2 + 2Na^+ + 2^-OH$$

$$Zn^{2+} + 2^-OH \rightleftharpoons Zn(OH)_2$$

$$Zn(OH)_2 \rightleftharpoons ZnO + H_2O$$

$$Zn + 2NaHCO_3 \rightleftharpoons ZnO + 2CO_2 + 2Na\uparrow + H_2O$$

In general, $M + NaHCO_3 \rightleftharpoons MO + CO_2 + Na\uparrow + H_2O$

In basic solution, $SeO_4^{2-} \xrightarrow{0.03} SeO_3^{2-} \xrightarrow{-0.36} Se$

The overall reaction is, $Zn + Se \underset{}{\overset{NaHCO_3}{\rightleftharpoons}} Se\text{-doped } ZnO$

Scheme 1

2.2. Determination of Photocatalytic Activities

Indigo carmine dye (Molecular formula: $C_{16}H_8O_8N_2S_2$, Molecular weight: 466.16, Λ_{max} = 610 nm) solution (3×10^{-5} M) was prepared by dissolving in distilled water. This solution was used as a test contaminant for evaluating photocatalytic activities of the commercial and prepared ZnO and Se-doped ZnO nanoparticles. The investigation was carried out both under sunlight and UV-light in order to check the efficiency of Se-doped ZnO nanoparticles. To examine the photocatalytic activity, 20 ml of colloidal solution were transferred to centrifuge tube and centrifuged at 800 rpm to remove the dispersed catalyst and the percentage transmittance was recorded for the clear solution. The chemical oxygen demand was recorded both before and after degradation of the dye using dichromate oxidation method [22,23]. The decrease in COD (mg/l) and increase in %T of the dye solution with color removal was observed as follows;

Se-doped ZnO >ZnO>commercially available ZnO.

3. RESULTS AND DISCUSSION

3.1 UV-visible Spectra

UV-Visible spectrum (Fig. 2) of Se-doped ZnO over the range of 200-800 nm showed that the synthesized nanoparticles are photoactive under visible light irradiation. The band gap of Se-doped ZnO was calculated using Tauc plot (Fig. 3). For a semiconductor sample, it is possible to determine the optical absorption near the band edge by the equation, $\alpha h\nu = A(h\nu-E_g)^{n/2}$ where α, h, ν, E_g and A are absorption coefficients, plank's constant, radiation frequency, band gap and a constant respectively. The n value decides the characteristics of the transition in a semiconductor being 1 or 4 respectively, for a direct or an indirect semiconductor. In order to get an accurate value of the band gap of solids, it is neccesary to construct a $(\alpha h\nu)^{1/2}$ versus $h\nu$ also called Tauc plot [24]. The band gap energy could be thus

estimated to be 2.6 eV for Se-doped ZnO nanoparticles. Doping of Selenium to ZnO results a remarkable increase in the photocatalytic activity, because the electronic energy levels of these two substances match each other and hence the red shift. The red shift is due to two factors; one is Burstein-Moss shift making the optical band gap broaden, the other one is interactions among the carriers which result in a many-body effect causing the band gap to become smaller [25].
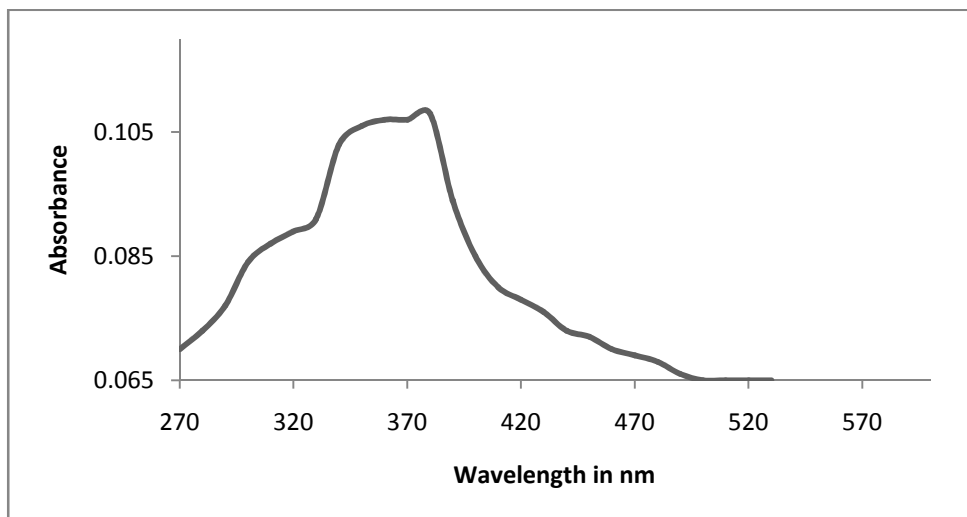

Fig. 2. UV-Visible spectra Se-doped ZnO nanoparticles

3.2 X-ray Diffraction

Fig. 4 represents the XRD patterns of Se-doped ZnO nanoaprticles. From the XRD data it is evident that Se-doped ZnO nanoparticles exhibit dominant diffraction peaks at 26.1788 (004), 29.9266 (101), 43.8478 (112), 46.0273 (112), 49.9094 (114) and 66.9720 (204) which were absent in ZnO [26]. The size was calculated using Williamson-Hall plot (Fig. 5) [27]. From this the crystallite size of Se-doped ZnO was found to be ~25.5 nm.

The XRD of ZnO and Se-doped ZnO nanoparticles are compared with ZnO nanoparticles and are as follows;

From the XRD data the cell parameters are calculated and it is found to be a = b ≠ c (a = 3.061 Å, b = 3.061 Å and c = 13.60 Å) and α = β = γ = 90^0. Accordingly, Se-doped ZnO nanoparticles belong to Tetragonal crystal system. The size for synthesized ZnO [27] nanoparticles calculated from Williamson- Hall plot was found to be ~7nm. From the XRD data the cell parameters are calculated and it is found to be a = b ≠ c (a = 8.143 Å, b = 8.143 Å and c = 5.005 Å) and α = β = γ = 90^0. Accordingly, ZnO nanoparticles belong to Tetragonal crystal system.
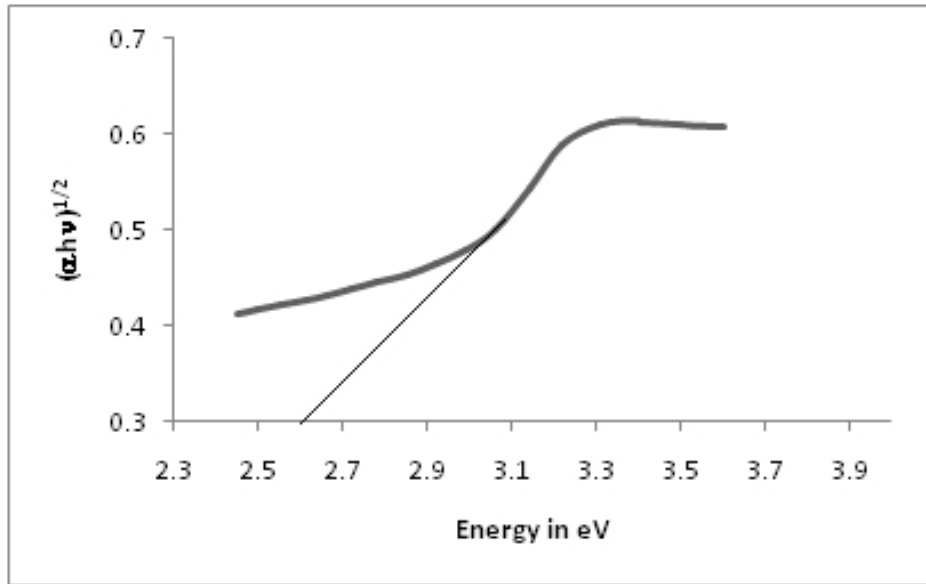
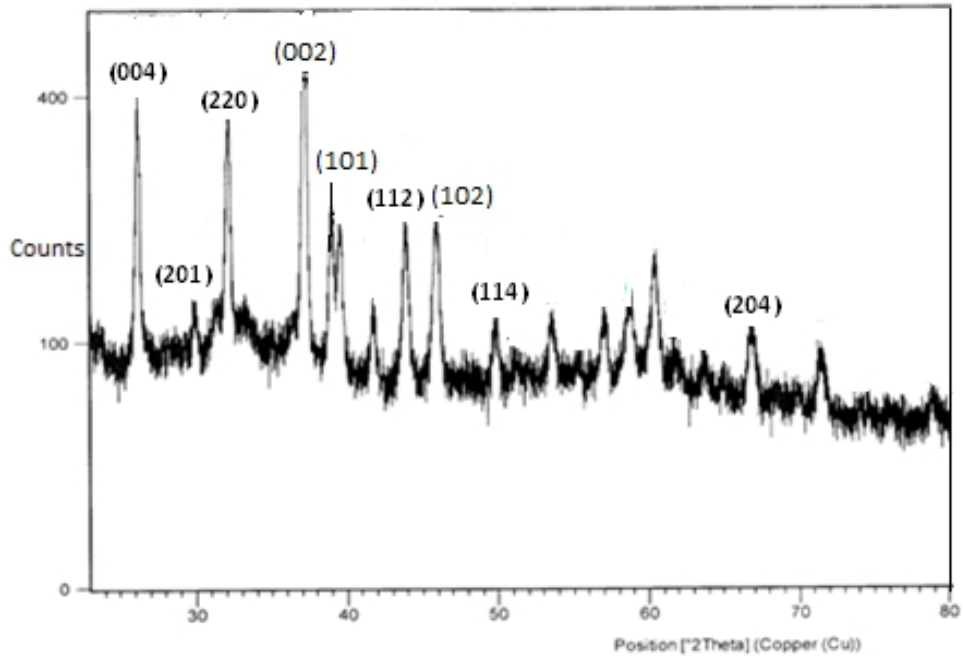**Fig. 3. Tauc plot of Se-doped ZnO nanoparticles**

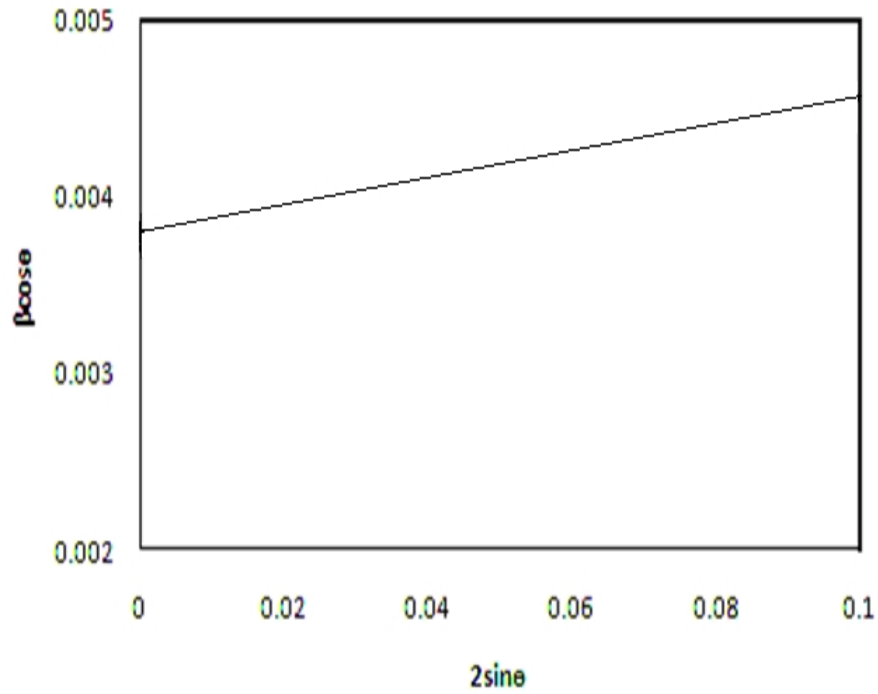**Fig. 4. XRD patterns of Se-doped ZnO nanoparticles.**

Fig. 5. Williamson-Hall plot.

3.3 Infra Red Spectra

IR spectrum of Se-doped ZnO is as shown in Fig. 6. Due to interionic vibrations, metal oxides generally give absorption bands below 1000 cm^{-1}. The peak at 427 cm^{-1} corresponds to Zn-O bonds. The presence of Se is confirmed with the appearance of the bands at 518 cm^{-1}, 612 cm^{-1}, 727 cm^{-1} and 1373 cm^{-1} which were absent for ZnO. The M-O frequencies observed for nanoparticles of metal oxides are in accordance with the literature values [25].
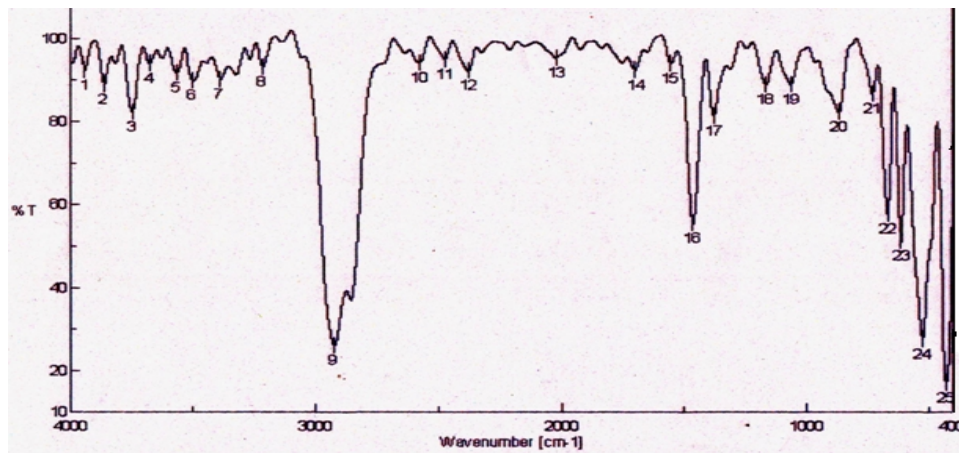

Fig. 6. IR spectrum of Se-doped ZnO nanoparticles

3.4 Scanning Electron Microscopy (SEM)

The surface morphology of the synthesized samples was observed by using SEM. The SEM micrographs (Fig. 7) of Se-doped ZnO samples show that it consists of agglomerated particles.
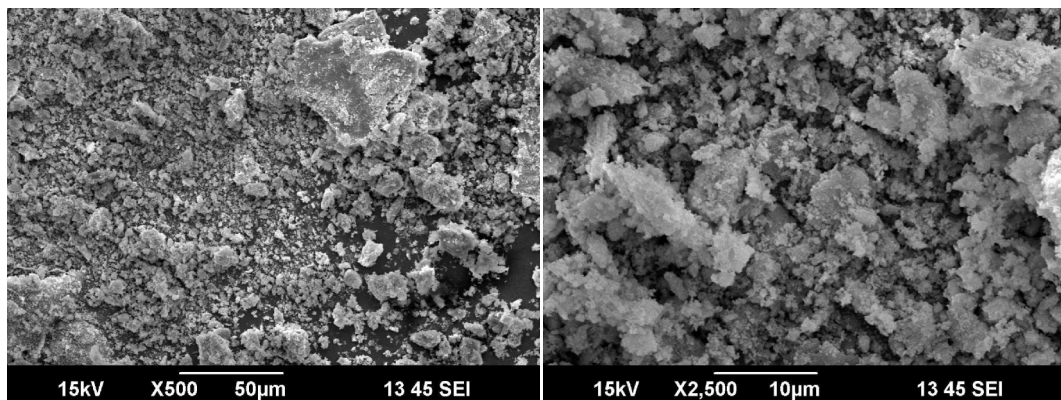

Fig. 7. SEM micrographs of Se-doped ZnO nanoparticles

3.5 Photodegradation Kinetics and COD Measurements

3.5.1 Effect of concentration of indigocarmine

The reaction was performed with different concentration of IC with constant weight of Se-doped ZnO catalyst. The change in concentration of the indigo carmine was recorded by change in color using spectrophotometer. A plot of log T_t (percentage transmittance of light) versus time was linear up to 60 % of the reaction indicating the disappearance of indigocarmine follows first order kinetics (Fig. 8). The rate constant values are given in Table 1 and the reaction rate decreased with increase in indigocarmine. This is because with increase in the dye concentration, the solution becomes more intense colored and the path length of the photons entering the solution is decreased thereby few photons reached the catalyst surface. Hence the production of hydroxyl radicals is reduced. Therefore the photodegradation efficiency is reduced. The pH and COD [28] for indigocarmine solution before and after degradation were measured and are given in Table 3. Results of COD effect are illustrated in Fig. 9.

Table 1. Effect of photodegradation at different concentration of indigo carmine

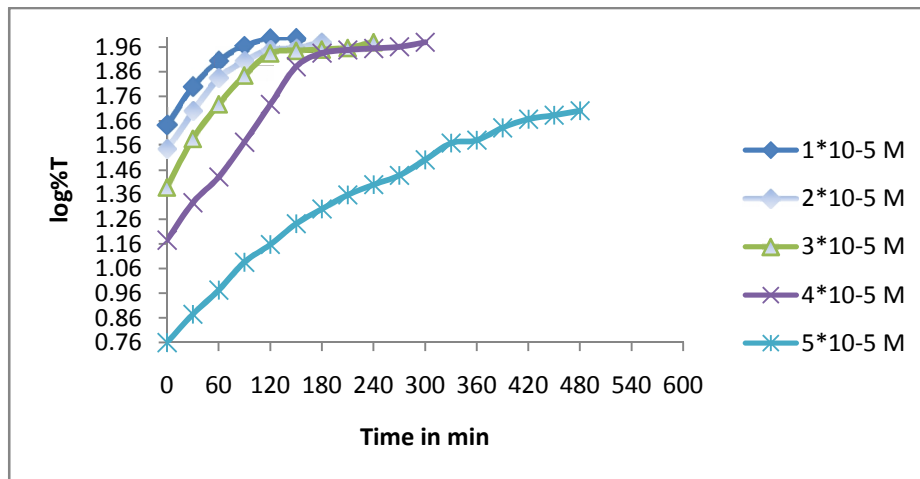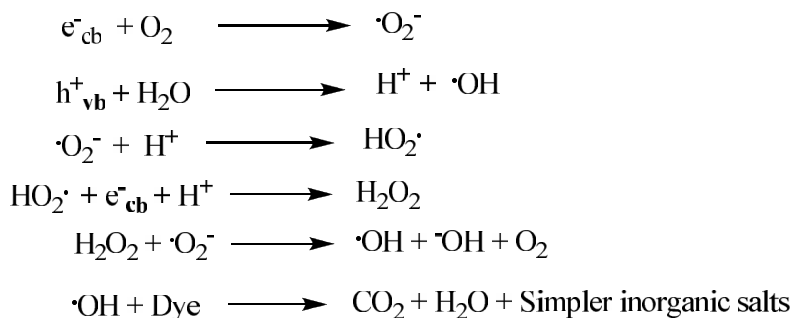| 10^{-5} [IC]	10^4 K Sec^{-1}	Effect of pH		COD values in mg/l	
		Before Degradation	**After Degradation**	**Before Degradation**	**After Degradation**
1.0	6.52	10.15	9.34	254	16
2.0	5.30	9.98	9.16	368	32
3.0	4.22	9.76	8.93	448	16
4.0	3.45	9.55	8.63	496	32
5.0	1.53	9.32	8.55	672	128

Fig. 8. Effect of concentration of IC on the rate of degradation

To account for mineralization COD was determined at different stage. The formation of different radical species during photodegradation is given in scheme 2.The dye was found to have mineralized into H_2O, CO_2 and simpler inorganic salts [29], after being irradiated for 5 hrs using Se-doped ZnO photocatalysts (Scheme 3). The photodegradation efficiency of the photocatalyst was calculated by the following formula,

$$Photodegradation\ efficiency = \frac{Initial\ COD - Final\ COD}{Initial\ COD} \times 100$$

$$e^-_{cb} + O_2 \longrightarrow {}^{\cdot}O_2^-$$

$$h^+_{vb} + H_2O \longrightarrow H^+ + {}^{\cdot}OH$$

$${}^{\cdot}O_2^- + H^+ \longrightarrow HO_2^{\cdot}$$

$$HO_2^{\cdot} + e^-_{cb} + H^+ \longrightarrow H_2O_2$$

$$H_2O_2 + {}^{\cdot}O_2^- \longrightarrow {}^{\cdot}OH + {}^-OH + O_2$$

$${}^{\cdot}OH + Dye \longrightarrow CO_2 + H_2O + Simpler\ inorganic\ salts$$

Scheme 2

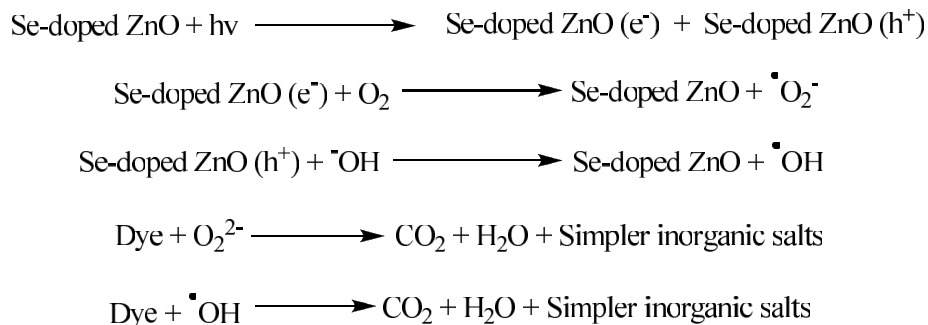### 3.5.2 Effect of pH

The pH of the solution is one of the important factors in evaluating the photodegradation reaction in aqueous medium. In the present work, the pH of the solution was adjusted by adding 0.01 M HCl solution. The effect of pH was studied at pH 4, pH 6 and pH 9.72 by keeping all other experimental conditions constant. The results are given in Fig. 10 and Table 2. From the results it is observed that, the rate of degradation increases from pH 4.0 to pH 9.72. Also, the amount of catalyst recovered after the experiment was lowered at lower pH because of the dissolution of the semiconductor oxides at very low pH values. Results of

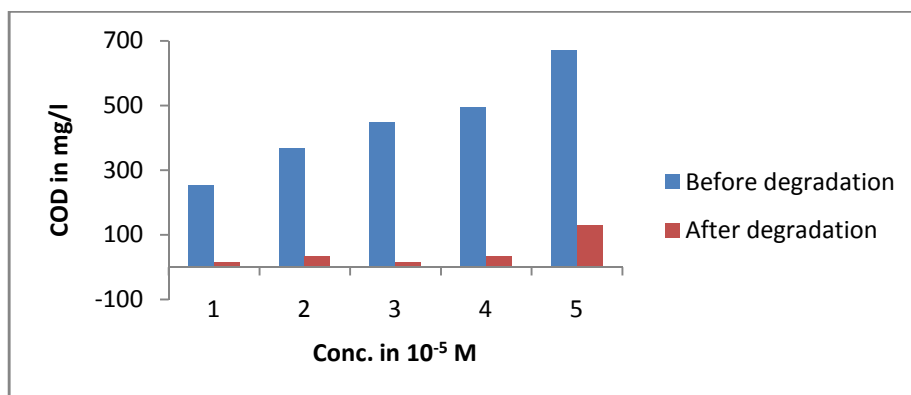COD effect are illustrated in Fig. 11. The optimum pH selected is 9.72 at which photodegradation is high.

$$\text{Se-doped ZnO} + h\nu \longrightarrow \text{Se-doped ZnO (e}^-) + \text{Se-doped ZnO (h}^+)$$

$$\text{Se-doped ZnO (e}^-) + O_2 \longrightarrow \text{Se-doped ZnO} + {}^\bullet O_2{}^-$$

$$\text{Se-doped ZnO (h}^+) + {}^- OH \longrightarrow \text{Se-doped ZnO} + {}^\bullet OH$$

$$\text{Dye} + O_2{}^{2-} \longrightarrow CO_2 + H_2O + \text{Simpler inorganic salts}$$

$$\text{Dye} + {}^\bullet OH \longrightarrow CO_2 + H_2O + \text{Simpler inorganic salts}$$

Scheme 3

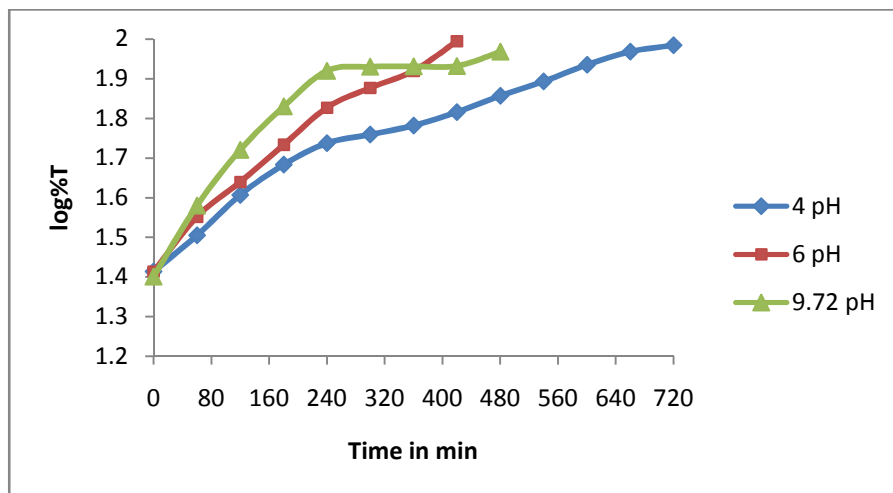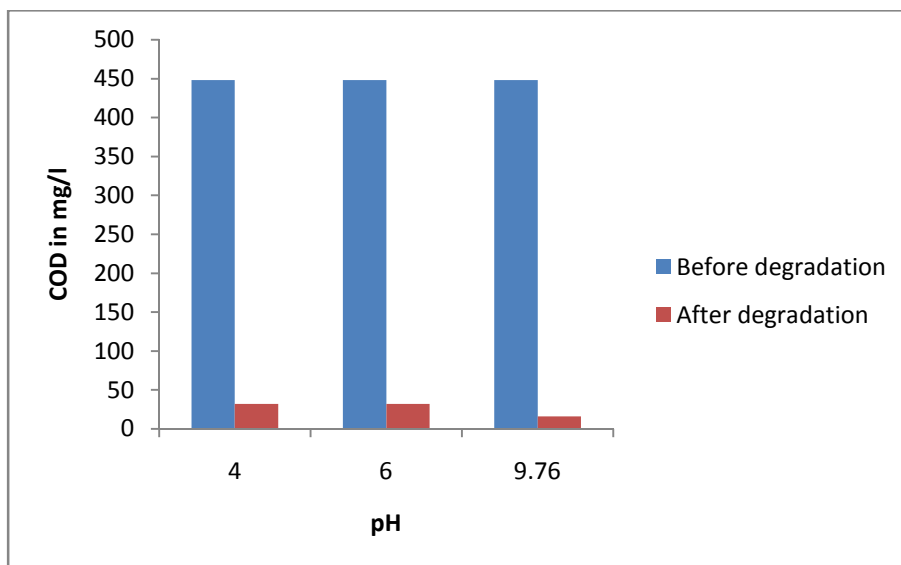**Fig. 9. Effect of concentration of IC on COD values**

Fig. 10. Effect of pH on the rate of degradation of IC

Table 2. Effect of pH on photodegradation of Indigo Carmine

pH	$10^4 k\ sec^{-1}$	COD values in mg/l		Photodegradation Efficiency %
		Before Degradation	**After Degradation**	
4.0	1.15	448	32	92.85
6.0	2.30	448	32	92.85
9.72	4.22	448	16	96.42

Fig. 11. Effect of pH on COD values

3.5.3 Effect of catalyst loading

The experiments were performed by taking different amount of catalyst varying from 10 mg-40 mg in order to study the effect of catalyst loading. The study showed that increase in catalyst loading from 10 mg-20 mg increased dye removal efficiency. Further increase in catalyst above 20 mg decreased the photoactivity of the catalyst. The reason for this decrease in degradation rate is due to the aggregation of Se-doped ZnO nanoparticles at high concentration causing a decrease in the number of surface active sites and increase the opacity and light scattering of Se-doped ZnO nanoparticles at high concentration. This tends to decrease the passage of light through the sample [30]. Further, the present study indicated, from economic point of view, the optimized photocatalyst loading is 20 mg/20 ml (Fig. 12 and Table 3). A result of COD effect is illustrated in Fig. 13.

3.5.4 Effect of light intensity

The above mentioned kinetic study of photodegradation of indigo carmine dye was studied under sunlight. The photodegradation rate with sunlight was compared with UV light (Figs. 14, 15 and Table 4). It is noticed that the photodegradation rate was increased in sunlight for prepared Se-doped ZnO than ZnO. This is because; the inclusion of Se^{2+} in ZnO matrix caused an decrease in the band gap of ZnO from 3.3 eV to 2.6 eV indicating that

these semiconductor nanoparticles absorb sunlight. This can subsequently activate these modified metal oxide photocatalysts upon sunlight irradiation. When a photon incident on a semiconductor (Se-doped ZnO) whose energy matches or exceeds the band gap energy of semiconductor, an e^- is ejected from valence band to conduction band, leaving a positively charged hole h^+ in the valence band. Excited state conduction band electrons and valence band holes can recombine and dissipate energy in the form of heat, get trapped in metastable surface states or react, respectively, with electron acceptors and donors that happen to be adsorbed on the semiconductor surface or within the surrounding electrical double layer of the charged nanoparticles. In the absence of suitable e^-/h^+ charged carriers the stored energy is dissipated within a few nanoseconds by recombination [31]. If a suitable scavenger or surface defect state is available to trap the electron or hole, recombination is prevented and subsequent redox reaction may occur. As there are many number of defect in Se-doped ZnO nanoparticles, electron or hole recombination is prevented and therefore Se-doped ZnO acts as a very good photocatalyst and is very active under sunlight compare to ZnO alone.
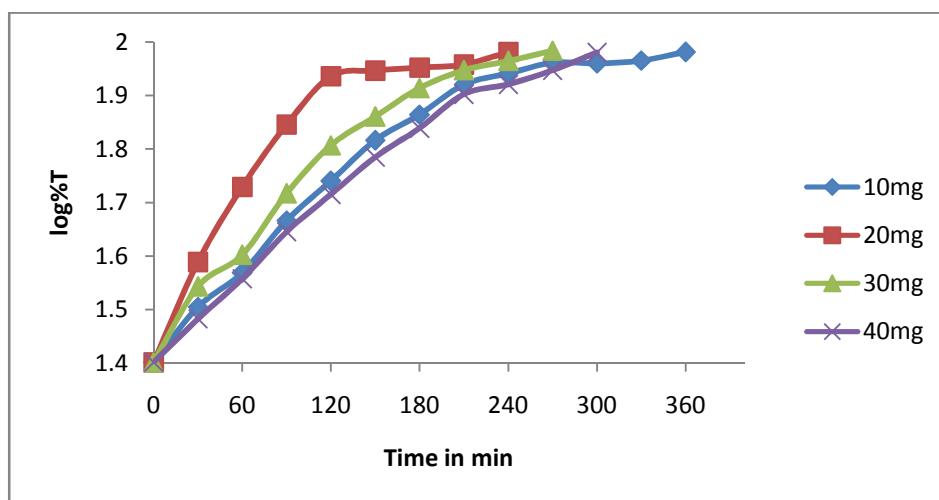

Fig. 12. Effect of catalyst loading on the rate of degradation of IC under sunlight

Table 3. Effect of catalyst loading on the photodegradation of Indigo Carmine under sunlight

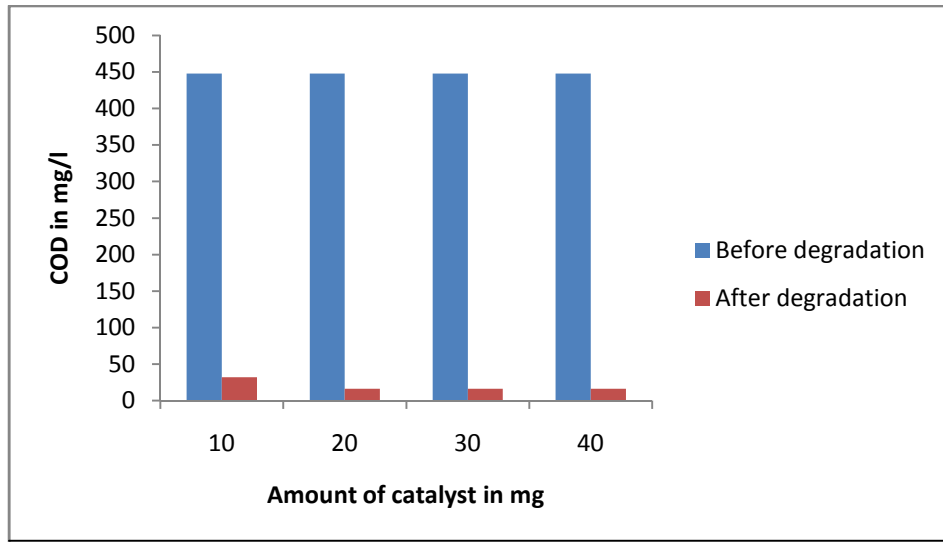| Catalyst (Se-doped ZnO) in mg	$10^4 K$ Sec^{-1}	Effect of pH		COD values in mg/l	
		Before Degradation	**After Degradation**	**Before Degradation**	**After Degradation**
10	2.68	9.70	8.79	448	32
20	4.22	9.76	8.93	448	16
30	3.83	9.69	8.96	448	16
40	3.07	9.70	8.86	448	16

Fig. 13. Effect of catalyst loading on COD values for the degradation of Indigo Carmine under sunlight
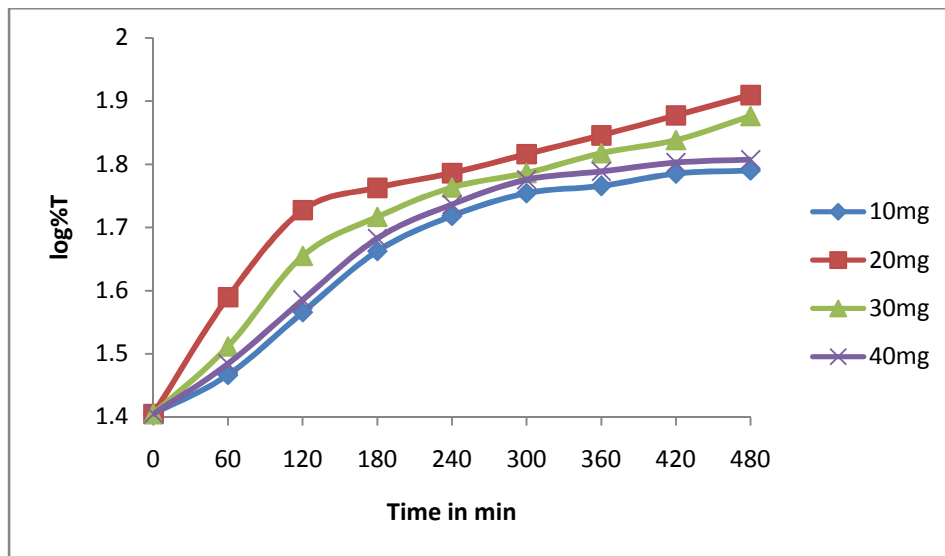

Fig. 14. Effect of catalyst loading on the rate of degradation of Indigo Carmine under UV light

3.5.5 Reuse of catalyst

The possibility of reusing the photocatalyst was tested to see the cost effectiveness of the method. After the degradation of the dye, the dye solution was kept standing for 10 hrs and then the supernatant liquid was decanted. The photocatalyst was thoroughly washed with double distilled water and then reused for the photodegradation by taking fresh dye solution.

From the degradation study it was observed that the efficiency of the catalyst to degrade the dye solution was slightly reduced to approximately 80 % for the use of 2 to 3 times. Further use of the catalyst showed lesser efficiency.

Table 4. Effect of catalyst loading on the photodegradation of Indigo Carmine under UV light

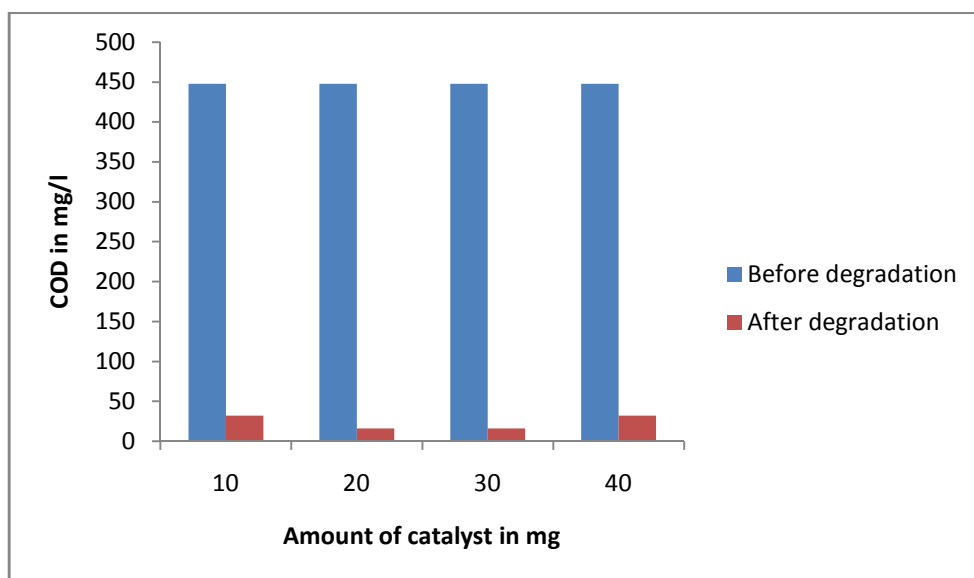| Catalyst (Se-doped ZnO) in mg	10^4K Sec^{-1}	Effect of pH		COD values in mg/l	
		Before Degradation	**After Degradation**	**Before Degradation**	**After Degradation**
10	1.91	9.62	8.69	448	32
20	3.07	9.73	8.83	448	16
30	2.68	9.61	8.94	448	16
40	2.30	9.68	8.88	448	32

Fig. 15. Effect of catalyst loading on COD values for the degradation of Indigo Carmine under UV light

4. BIOLOGICAL ACTIVITIES

4.1 Antimitotic Activity

Cell is the basic structural, functional and biological unit of living organisms. They are called building blocks of life. Cell division involves a single cell (called a mother cell) dividing into two daughter cells. Between successful cell division, cell grow through the functioning of cellular metabolism and is responsible for the development of organisms [32].

Allium cepa has been used to evaluate the antimitotic activity of synthesized ZnO and Se-doped ZnO nanoparticles. Results of antimitotic activity are given in Table 5, the different stages of mitosis (Fig. 16), the percentage inhibition of cell division by ZnO and Se-doped

ZnO nanoparticles comparative to control is given in Fig. 17. It can be clearly seen that there exists a changes in cellular morphology such as slight elongation in shape with many of them remains in the earliest stages of mitosis called prophase stage in Se-doped ZnO and cell growth inhibition is less effectively effected in ZnO compared to control. Onion roots in ZnO and Se-doped ZnO of concentration (25, 50 and 75 ppm) at different time duration (12, 18 and 24 hrs) exhibited changes in chromosomes and shape of the cells with elongated appearance. Change in chromosomes and cellular morphology were achieved in increasing time and concentration. Se-doped ZnO showed good inhibitory effect by inhibiting the cell growth and ZnO showed moderate inhibition towards cell division.

From the above observations, the partial-c-mitosis, full-c-mitosis with partial functional spindles and comparatively normal mitotic cells phases were noticed in various cells of the same root tip between 12-24 hrs time duration. Hence, Se-doped ZnO has very good ability in controlling the cell division.
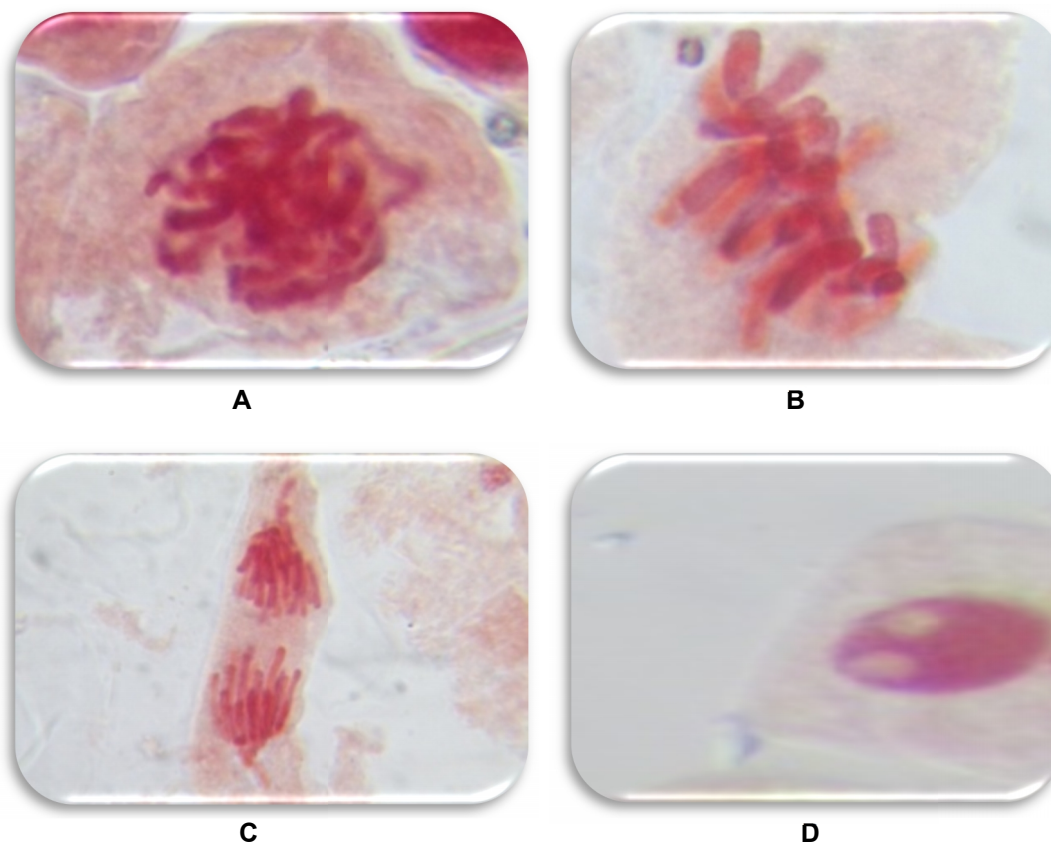

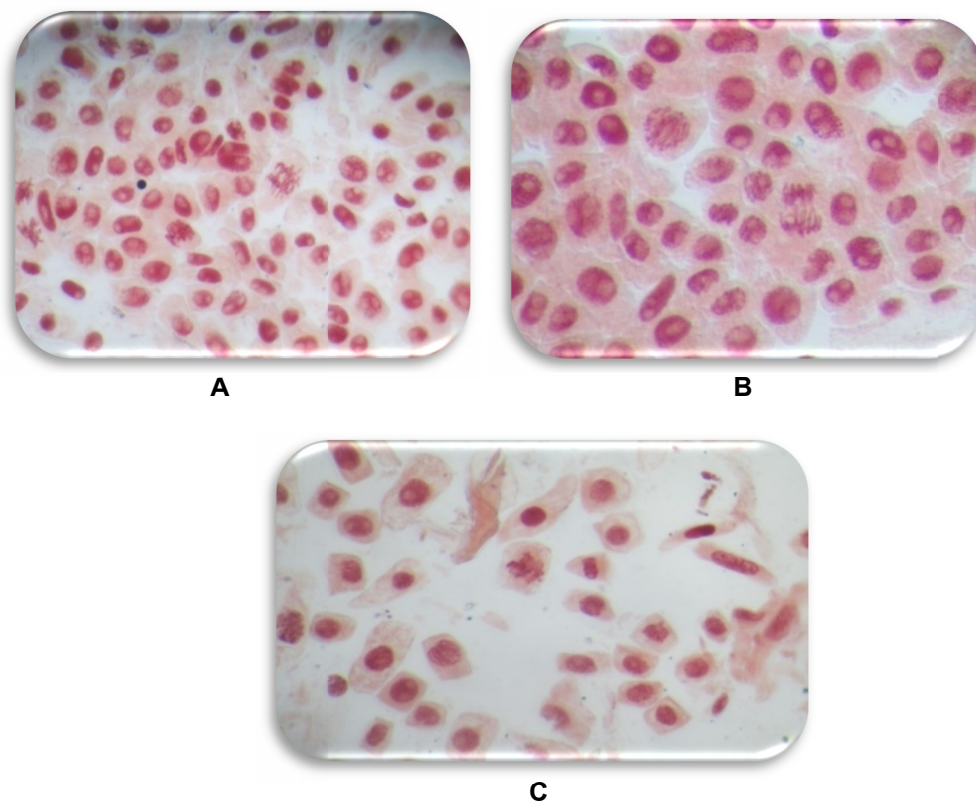**Fig. 16. A) Prophase; B) Anaphase; C) Metaphase; and D) Telophase**

Fig. 17. Cell growth inhibitions by Control (A), ZnO (B) and Se-doped ZnO (C) nanoparticles

4.2 Antimicrobial Activity

The antibacterial activity of ZnO and Se-doped ZnO nanoparticles was evaluated by well diffusion method. The study was subjected to evaluate the ability of these nanoparticles as antibacterial agent against five bacterial strains which are well known to cause some infections to humans namely, *E. fecalis, K. pneumonia, E. aerugenes, P. aerugenosa, A. fecalis*. The antibacterial activity was evaluated by measuring the zone of inhibition in mm (Table. 6). The effect of antibacterial activity by ZnO and Se-doped ZnO nanoparticles against *E. fecalis* bacterial strain is as shown in Fig. 18. The results of antibacterial activity of ZnO and Se-doped ZnO nanoparticles are given in Table 6. The biggest inhibition was observed with Se-doped ZnO, for the growth of *E. fecalis* is similar to standard Chloromphenicol. Further, around 80-90 % of inhibition was observed for *K. pneumonia* and *P. aerugenosa* by Se-doped ZnO. ZnO nanoparticles were also shown good antibacterial activity but less when compared to Se-doped ZnO nanoparticles.

Synthesized ZnO and Se-doped ZnO nanoparticles were also screened to evaluate their antifungal activity against *Fusarium and Aspergillus*. Again, very good inhibition was recorded for Se-doped ZnO against fungi *Fusarium* and *Aspergillus*, while ZnO records the moderate zone of inhibition against tested fungi (Fig. 19, Table 7).

Table 5. Effect of ZnO and Se-doped ZnO nanoparticles on antimitotic activity

Compound	Conc. in PPM	% Dividing cells			% of Dividing Cell Compare to Control			% of Inhibition Compare to Control		
		12 hrs	18 hrs	24 hrs	12 hrs	18 hrs	24 hrs	12 hrs	18 hrs	24 hrs
Control		74.57	84.16	82.59	100	100	100	00	00	00
	25	64.57	69.32	67.54	86.68	82.36	81.77	13.41	17.63	18.22
ZnO	50	59.32	62.42	64.02	79.54	74.16	77.51	20.45	25.83	22.48
	75	54.79	65.97	59.54	73.47	78.38	72.09	26.52	21.61	27.90
	25	55.80	54.75	64.04	74.82	65.05	77.53	25.17	34.94	22.46
Se-doped ZnO	50	51.32	52.30	60.34	68.82	62.14	73.05	31.17	37.85	26.94
	75	47.16	47.15	54.75	63.24	56.02	66.29	36.75	43.97	33.70

Table 6. Effect of ZnO and Se-doped ZnO nanoparticles on antibacterial activity

Compound No.	Zone of Inhibition in mm				
	Enterococcus faecalis	*Klebsiella pneumonia*	*Enerobacter aerugenes*	*Pseudomonas aeruginosa*	*Alcaligenes faecalis*
Conc. in mg/ml	0.1	0.1	0.1	0.1	0.1
Control (solvent)	00	00	00	00	00
Chloromphenicol	18.4±0.08	18.8±0.06	19.2±0.04	18.6±0.06	18.4±0.03
ZnO	03.4±0.05	05.2±0.02	04.8±0.04	08.2±0.05	05.0±0.04
Se-doped ZnO	18.4±0.15	15.2±0.04	11.4±0.04	16.6±0.08	12.4±0.08

Fig. 18. Antibacterial activity of ZnO (1a) and Se-doped ZnO (1b) against *E. fecalis* bacterial strain
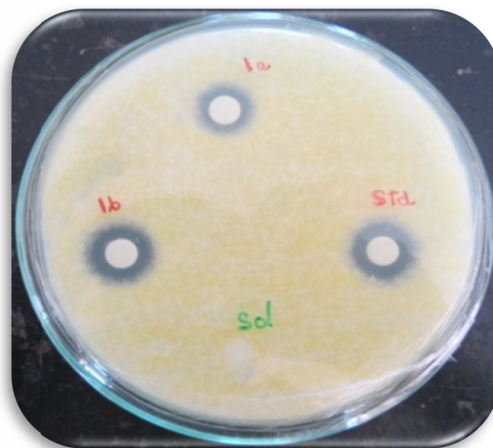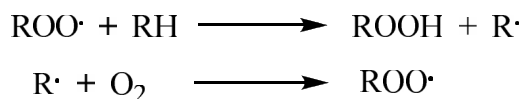

Fig. 19. Antifungal activity of ZnO and Se-doped ZnO against *Fusarium* and *Aspergillus* bacterial strain

Table 7. Effect of ZnO and Se-doped ZnO nanoparticles on antifungal activity

Compound No.	Zone of Inhibition in mm	
	Fusarium verticillioides	*Aspergillus flavus*
Conc. in mg/ml	0.1	0.1
Control	00	00
Nystatin	22.0±0.04	18.0±0.06
ZnO	12.2±0.04	08.1±0.04
Se-doped ZnO	16.2±0.04	12.4±0.02

4.3 The Potent Activity of Se-doped ZnO and ZnO

The potent activity of Se-doped ZnO is explained as follows; Some of the differences in the cell growth are related to the modest changes observed in surface energy, hydrophilicity and hydrophobicity upon Se doping, compared to undoped ZnO and control. Control tissue fractions consume O_2 at a more rapid rate, hence higher the chain reaction and cell growth.

$$ROO^{\cdot} + RH \longrightarrow ROOH + R^{\cdot}$$

$$R^{\cdot} + O_2 \longrightarrow ROO^{\cdot}$$

The presence of Se may act as antioxidant scavenging for free radical intermediates ($ROO^{\cdot}$, $^{\cdot}OH$, etc...), thereby breaking the chain reaction. Therefore the presence of nanoparticles could react with the radicals and gives considerably more stable compound, so that the cell viability is reduced with increase of cell death and hence inhibits the cell growth. However ZnO alone shows less inhibiting effect compared to Se-doped ZnO as it shows lesser antioxidant activity.

From the literature obtained the toxicity of the ZnO nanoparticles or Se nanoparticles were observed for the concentration greater than 500 ppm [33-36], which is much higher than the concentration of nanoparticles used in our present study, whose concentration varies from 25ppm-100 ppm. Hence the synthesized nanoparticles may be considered safe up to concentration of 200 ppm.

5. CONCLUSION

Se-doped ZnO nanoparticles were synthesized by electrochemical method, an environmentally friendly method. Photodegradation by these semiconductors offers a green technology for the removal of hazardous compounds present in the industrial effluents. Kinetics for the degradation of Indigocarmine by Se-doped ZnO nanoparticles were studied systematically. The completion of degradation reaction was confirmed by conducting COD experiment. Results of COD effect revealed that ~96 % of the dye has been degraded. The synthesized nanoparticles are capable of entering into the allium cepa cell, bacterial cell, fungus cell, therefore inhibits the cell growth and hence confirms the biological activity as a potent antimitotic and antimicrobial agents. The synthesized nanoparticles may be safe up to the concentration of 200 ppm.

ACKNOWLEDGEMENTS

COMPETING INTERESTS

Authors have declared that no competing interests exist.

REFERENCES

1. Sahoo SK, Parveen S, Panda JJ. The present and future of nanotechnology in human health care. Nanomed. 2007;3:20-31.

2. Doria G, Conde J, Veigas B, Giestas L, Almeida C, Assuncao M, Rosa J, Baptista PV. Noble metal nanoparticles for biosensing applications. Sensors. 2012;12:1657-1687.

3. De Gusseme B, Sintubin L, Baert L, Thibo E, Hennebel T, Vermeulen G, Uyttrendaele M, Verstraete W, Boon N. Biogenic silver nanoparticles for disinfection of viral contaminated water. Commun. Agric Appl Biol Sci. 2011;76:73-76.

4. El-Sayed MA. Some interesting properties of metals confined in time and nanometer space of different shapes. Acc Chem Res. 2001;34:257–264.

5. McConnell WP, Novak JP, Brousseau LC, Fuierer RR, Tenent RC, Feldheim DLJ. Electronic and optical properties of chemically modified metal nanoparticles and molecularly bridged nanoparticle arrays. Phys Chem B. 2000;104:8925–8930.

6. Liu C, Zhang ZJ. Size-dependent superparamagnetic properties of Mn spinel ferrite nanoparticles synthesized from reverse micelles. J Chem Mater. 2001;13:2092–2096.

7. Moreno-Man˜as M, Pleixats R. Formation of carbon–carbon bonds under catalysis by transition-metal nanoparticles. Acc Chem Res. 2003;36:638–643.

8. Boen H, Chen-Ju H. Structure and properties of Ag embedded Al doped ZnO nanocomposite thin films prepared through a sol-gel process, Surface abd coatings technology. Surface and Coatings Technology. 2006;201:3188-3192.

9. Clark LC, Combs GF, Turnbull BW, Slate EH, Chalker DK, Chow J, Davis LS, Glover RA, Graham GF, Gross EG, Krongard A, Lesher JL, Park HK, Sanders B, Smith CL, Taylo JR. Effect of selenium supplementation for cancer prevention in patients with carcinoma of the skin. J Am Med Assoc. 1996;276:1957–1963.

10. Fernandez BF, Cabre E, Esteve M, Mingorance MD, Abad LA, Lachica M, Gil A, Gassull MA. Serum selenium and risk of large size colorectal adenomas in a geographical area with a low selenium status. Am J Gas Ent. 2002;97:2103–2108.

11. Nelson MA, Reid M, Duffield-Lillico AJ, Marshall JR. Prostate cancer and selenium. Urol Clin N Am. 2002;29:67–70.

12. Davis CD, Zeng H, Finley JW. Selenium-enriched broccoli decreases intestinal tumorigenesis in multiple intestinal neoplasia mice. J Nutr. 2002;132:307–309.

13. Ip C, Birringer M, Block E, Kotrebai M, Tyson JF, Uden PC, Lisk DJ. Chemical speciation influences comparative activity of selenium-enriched garlic and yeast in mammary cancer prevention. J Agric Food Chem. 2000;48:4452-4452.

14. Phong A Tran, Thomas J Webster, Selenium nanoparticles inhibit *Staphylococcus aureus* growth. International Journal of Nano Medicine. 2011;6:1553-1558.

15. Klein EA. Selenium: Epidemiology and basic science. J Urol. 2004;171(2):503-53.

16. Helzlsouer KJ, Huang HY, Alberg AJ, Hoffman S, Burke A, Norkus EP, et al. Association between alpha-tocopherol, gamma-tocopherol, selenium and subsequent prostate cancer. J Natl Cancer Inst. 2000;92(24):2018-2023.

17. Ling Konga, Qing Yuana B, Huarui Zhua, Ying Li C, Quanyi Guo D, Qin Wang B, Xiaolin Bi A, Xueyun Gaoa. The suppression of prostate LNCaP cancer cells growth by Selenium nanoparticles through Akt/Mdm2/AR controlled apoptosis, Biomaterials. 2011;32:6515-6522.

18. Song XC, Zheng YF, Yang E, Liu G, Zhang Y, Chen HF, Zhang YY. Photocatalytic activities of Cd doped $ZnWO_4$ nanorods prepared by a hydrothermal process. J Haz Mat. 2010;179:1122-1127.

19. Bandara J, Kuruppu SS, Pradeep UW. The promoting effect of MgO layer in sensitized photodegradation of colorants on TiO_2/MgO composite oxide. Collides and surfactants A: Physicochem Eng Aspects. 2006;276:197-202.

20. Nyffenegger RM, Craft B, Shaaban M, Gorer S, Erley G, Penner RM. A hybrid electrochemical/chemical synthesis of Zinc oxide nanoparticles and optically intrinsic thin films. Chem Mater. 1998;10:1120-1129.

21. Annal Therese GH, Vishnu Kamath P. Electrochemical synthesis of metal oxides and hydroxides. Chem Mater. 2000;12:1195-1204.

22. Chaitanya Lakshmi G, Ananda S, Somashekar, Ranganathaiah C. Synthesis of ZnO/ZrO_2 nanocomposites by electrochemical method and photocatalytic degradation of Fast green dye, paper dyeing and printing press effluent. Int J Adv Mater Sci. 2012;3:221-237.

23. Byrappa K, Subramani AK, Ananda S, Rai KML, Dinesh R, Yoshimura M. Photocatalytic degradation of rhodamine B dye using hydrothermally synthesized ZnO. Bull Mater Sci. 2006;29:1-6.

24. Belever C, Adan C, Fernandez-Garcia M. Photocatalytic behavior of Bi_2O_6 polymetalates for rhodamine B degradation. Catalysis today. 2009;143:274-281.

25. Venkatachalam N, Palanichany M, Banumathi A, Murugesan V. Enhanced photocatalytic degradation of 4-Chlorophrnol by Zr^{4+} doped nano Tio_2. J Mol Cata A: Chemical. 2007;266:158-165.

26. Shah Chetan P, Singh Krishan K, Kumar Manmohan, Bajaj Parma N. Vinyl monomers-induced synthesis of polyvinyl alcohol-stabilized selenium nanoparticles. Materials Research Bulletin. 2010;45:56-62.

27. William GK, Hall WH. X-ray line broadening from field aluminium and wolfram. Acta Metallurgica. 1953;1:22-31.

28. Byrappa K, Subramani AK, Ananda S, Rai KML, Dinesh R, Yoshimura M. Photocatalytic degradation of rhodamine B dye using hydrothermally synthesized ZnO. Bull Mater Sci. 2006;29:1-6.

29. Wei L, Shifu C, Wei Z, Sujuan Z. Titanium dioxide mediated photocatalytic degradation of methamidophos in aqueous phase. Journal of Hazardous materials. 2009;164:154-160.

30. Yadav MK, Ghosh M, Biswas R, Raychaudhuri AK, Mookerjee A. Band gap variation in Mg- and Cd-doped ZnO nanostructures and molecular clusters. Phy Rev B. 2007;76:1-9.

31. Chaitanya Lakshmi G, Ananda S, Somashekar, Ranganathaiah C. Synthesis of ZnO/MgO nanocomposites by electrochemical method and photocatalytic degradation kinetics of Eosin Yellow Dye. Int J Nanosci Nanotech. 2012;3:47-63.

32. Sehgal R, Roy S, Kumar VL. Evaluation of cytotoxic potential of latex of Calotropis procera and Podophyllotoxin in Allum cepa root model. Biocell. 2006;30:9-13.

33. Phong A Tran, Love Sarine, Robert H Hurt, Thomas J Webster. Differential effects of nanoselenium doping on healthy and cancerous osteoblasts in culture on titanium. International Journal of nanomedicine. 2010;5:351-358.

34. Hamilton JW, Tappel AL. Lipid antioxidant activity in tissues and proteins of Selenium-fed animals. The Journal of Nutrition. 1963;79:493-502.

35. Bijan Zare, Babaie S, Neda Setayesh, Ahmad Reza Shahverdi. Isolation and characterization of a fungus for extracellular synthesis of small selenium nanoparticles. Nanomedicine Journal. 2013;1:14-20.

36. Zong-Hong Lin, Fu-Chu Lin, Chris Wang CR. Observation in the growth of Selenium Nanoparticls. Journal of the Chinese Chemical Society. 2004;51:239-242.